European Journal of Pharmaceutics and Biopharmaceutics 205 (2024) 114535

Contents lists available at ScienceDirect

European Journal of Pharmaceutics and Biopharmaceutics

journal homepage: www.elsevier.com/locate/ejpb

Development of transferosomes for topical ocular drug delivery of curcumin

Geisa Nascimento Barbalho [a,b,1], Stefan Brugger [a,1], Christian Raab [c], Jara-Sophie Lechner [c], Taís Gratieri [b], Cornelia M. Keck [c], Ilva D. Rupenthal [a], Priyanka Agarwal [a,*]

[a] Buchanan Ocular Therapeutics Unit, Department of Ophthalmology, Aotearoa-New Zealand National Eye Centre, Faculty of Medical and Health Sciences, The University of Auckland, Auckland 1142, New Zealand
[b] Laboratory of Food, Drugs and Cosmetics (LTMAC), University of Brasilia, Brasilia 70910-900, DF, Brazil
[c] Department of Pharmaceutics and Biopharmaceutics, Philipps-Universität Marburg, Robert-Koch-Str. 4, 35037 Marburg, Germany

ARTICLE INFO

Keywords:
Ocular drug delivery
Liposomes
Transferosomes
Cornea
Curcumin

ABSTRACT

Background: Transferosomes (TFS) are ultra-deformable elastic bilayer vesicles that have previously been used to enhance gradient driven penetration through the skin. This study aimed to evaluate the potential of TFS for topical ocular drug delivery and to compare their penetration enhancing properties in different ocular tissues.
Methods: Curcumin-loaded TFS were prepared using Tween 80 as the edge activator. Drug release and precorneal retention of the TFS were evaluated in vitro, while their ocular biocompatibility and bioavailability were evaluated ex vivo using a curcumin solution in medium chain triglycerides as the oily control.
Results: The TFS had a narrow size distribution with a particle size less than 150 nm and an entrapment efficiency greater than 99.96 %. Burst release from the TFS was minimal and the formulation showed good corneal biocompatibility. Moreover, enhanced corneal and conjunctival drug penetration with significantly greater and deeper drug delivery was observed with TFS.
Conclusion: TFS offer a promising platform for ocular delivery of hydrophobic drugs. This study, for the first time, elucidates the effect of tissue morphology and osmotic gradients on drug penetration in different ocular tissues.

1. Introduction

The past few decades have seen significant advancement in drug delivery strategies with an ever-increasing focus on lipid-based nanotechnologies. Liposomes are one of the most extensively studied lipid-based nanoparticulate systems, since their rigid bilayer structure provides a versatile platform for delivery of both hydrophilic and lipophilic drugs [1,2]. Meanwhile, transferosomes (TFS) are elastic bilayer vesicles that further extend the drug delivery capability of liposomes [3–5]. Transferosomes are structurally similar to liposomes, but the bilayer structure is rendered elastic by incorporation of an "edge-activator", which may be a surfactant, such as Tween® 80 and Span® 80, or a bile acid, such as sodium cholate, that significantly reduces the elastic modulus of the phospholipid backbone [5–7]. The ultra-deformable and stress-responsive properties of TFS have been shown to facilitate skin penetration due to their ability to undergo reversible deformation and squeeze through intercellular pores that are smaller than their vesicle size [7–9]. Moreover, the high surface hydrophilicity of TFS facilitates their penetration along the osmotic gradient via "transpore hydrotaxis" which enhances their migration from the lipophilic epidermis to the richly perfused hydrophilic dermis [10,11]. Thus, their application in non-invasive drug delivery to the skin has been extensively explored [11,12].

While the mechanism of topical drug delivery to the skin and the eye is often presumed to be identical, ocular tissues are more susceptible to excipient related toxicity; therefore, the choice and concentration of excipients are significantly constrained in ocular drug delivery systems. Currently, the application of TFS in ocular drug delivery is limited to a handful of studies. Uwaezuoke et al. [13] hypothesized that osmotic gradients across the corneal epithelium and stroma are similar to those observed across the epidermis and dermis and evaluated corneal permeability and flux of TFS using different edge activators. Nanda et al. [14] prepared elastic vesicles using sodium deoxycholate as the edge activator and suspended them in a Carbopol gel for sustained drug

* Corresponding author.
E-mail address: p.agarwal@auckland.ac.nz (P. Agarwal).
[1] Joint first authors.

https://doi.org/10.1016/j.ejpb.2024.114535
Received 15 August 2024; Received in revised form 9 October 2024; Accepted 15 October 2024
Available online 18 October 2024

delivery of the antifungal drug, fluconazole, for the treatment of keratomycosis. Meanwhile, Mazyed et al. [15] prepared acetazolamide "transgelosomes" using different edge activators, including Tween 80, Span 60, and Cremophor RH 40, and incorporated them into poloxamer gels for a sustained therapeutic effect in the eye.

Although preliminary studies suggest that TFS can enhance corneal drug delivery, it is worth noting that the epithelial morphology and hydrophilic-lipophilic balance in different ocular tissues differ considerably [16,17]. The corneal epithelium is known to be the primary barrier to ocular drug delivery with tight intercellular junctions [18,19]. Meanwhile, the conjunctival epithelium has larger intercellular pores and is relatively hydrophilic [20,21]. Since the capability of TFS as drug carriers largely depends upon the tissue morphology with intercellular junction size and osmotic gradients across the tissue having a significant influence on TFS penetration [5,10], it may be hypothesized that their penetration and distribution in the corneal and conjunctival tissues will differ considerably. To test this hypothesis, this study aimed to compare TFS penetration in the cornea and bulbar and tarsal conjunctiva using curcumin as the model hydrophobic drug.

Curcumin is the major curcuminoid obtained from the rhizomatous plant, turmeric (*Curcuma longa*), that has extensively been studied for its anti-oxidant and anti-inflammatory activities. Curcumin's application in the management of several ocular inflammatory conditions, such as dry eye disease [22], allergic conjunctivitis [23], uveitis [24,25], cataract [26], diabetic retinopathy [27] and proliferative vitreoretinopathy [28] has previously been demonstrated. However, curcumin is very lipophilic with a Log P of 4.16 and three pKa values of 8.38 ± 0.04, 9.88 ± 0.02 and 10.51 ± 0.01 due to which it remains virtually unionized and practically insoluble in water at physiological conditions [29–31]. Due to its poor aqueous solubility (11 ng/ml in aqueous buffer at pH 5) and cellular permeability, curcumin is classified as a biopharmaceutical classification system (BCS) class IV molecule [30,32]. As such, the biomedical potential of curcumin remains largely unexploited due to the difficulty encountered in delivering therapeutically relevant concentrations of curcumin. At present, there is no marketed ocular formulation of curcumin.

Here, we prepared and characterized phospholipid TFS using Tween 80 as the edge activator in a non-occlusive vehicle. Ocular biocompatibility and bioavailability of the TFS was evaluated using a conventional oily solution of curcumin in medium chain triglycerides (MCT) as the control. An advantage of using curcumin as the model drug was that its fluorescent nature facilitated drug visualisation and quantification in tissue layers by fluorescence microscopy. Thus, drug penetration and distribution in different ocular tissues, including the cornea, bulbar and tarsal conjunctiva, were compared to elucidate the transepithelial osmotic gradient driven diffusion of TFS across these tissues.

2. Materials and methods

2.1. Materials

Curcumin powder (*Curcuma longae pulvis*) was purchased from Receptura Apotheke, Germany. Medium chain triglycerides (MCT Labrafac Lipophile WL 1349) and Phospholipon 90 G were gifted by Gattefosse and Lipoid GmbH, Germany, respectively. Tween 80, chloroform and methanol were purchased from Merck, Germany. Milli-Q water, obtained by reverse osmosis using a Millipak system (0.22 μm; Millipore, USA) was used for TFS preparation and for all analyses. Isopropyl alcohol was purchased from Macron Fine Chemicals, Netherlands, while HPLC grade acetonitrile and methanol were purchased from J. T. Baker, USA. To prepare the polymeric films for the precorneal retention studies, poly-vinyl alcohol (PVA; 87–90 % hydrolyzed, molecular weight 30,000–70,000), mucin type II, and poloxamer 407 were purchased from Sigma-Aldrich, Germany, while gelatin was obtained from Vetec (Rio de Janeiro, Brazil). For the simulated tear fluid (STF), $NaHCO_3$ was obtained from ECP Labchem, New Zealand, and NaCl and $CaCl_2$ were purchased from Scharlau Chemicals, Spain.

2.2. Preparation of transferosomes

TFS were prepared using Phospholipon 90 G (phospholipid) and Tween 80 (edge activator) by the thin-film hydration technique described previously [33,34]. Briefly, the phospholipid film was prepared in an Eppendorf tube by dissolving 90 mg Phospholipon 90 G and 10 mg Tween 80 in 10 ml of organic solvent (methanol:chloroform, 1:2 (v/v)). The organic solution was transferred to a round bottom flask by rinsing with an additional 3 ml of organic solvent, and evaporated in a rotary evaporator (75 rpm, 35 °C, 320 mbar; Rotavapor R-215, Büchi, Switzerland), after which the films were dried under nitrogen for 5 min, covered in foil and stored in a vacuumed desiccator overnight. The dry films were rehydrated with 5 ml of Milli-Q water, preheated to 35 °C, and sonicated with a probe sonicator (UW2070, Bandelin Electronic, Germany) for 2 min at 40 % intensity (0.4 cycles) [35].

Curcumin-loaded TFS were prepared by adding varying amounts of curcumin (2.5, 5.0, 7.5, 10.0 or 15.0 mg) to 90 mg Phospholipon 90 G and 10 mg Tween 80 in 10 ml of organic solvent followed by evaporation in the rotary evaporator as described above. A 1 ml syringe extruder fitted with a 0.2 μm polycarbonate hydrophilic membrane (Nuclepore, Whatman, USA) was used for ten extrusions per ml. Drug loading (%) was calculated as previously described by Rodriguez et al. [36] using the equation below:

$$Drug\ \ Loading(\%) = \frac{weight\ \ of\ \ drug\ \ in\ \ sample}{total\ \ weight\ \ of\ \ sample} \times 100$$

2.3. Particle size, polydispersity index and zeta potential

The particle size, polydispersity index (PDI) and zeta potential (ZP) were determined in triplicate by dynamic light scattering (DLS) and laser doppler anemometry (LDA) using a ZetaSizer NanoZS Zen3600 (Malvern Instruments, USA). Particle size and PDI were measured at 25 °C with an equilibration time of 120 s. Blank TFS were diluted 1:25 (v/v) in PBS, while the curcumin TFS were further diluted to a final concentration of 2:100 (v/v) to minimise any refractive error due to dye fluorescence.

The ZP of the TFS was measured using conductivity water (CW) for reproducibility, as described previously [37]. CW was prepared by boiling Milli-Q water in a 50 ml Schott bottle for 10 min and covering it with an unscrewed lid. Post-equilibration for 3 days, NaCl was added to obtain a conductivity of 50 μS/cm (Mettler Toledo, USA). Transferosomes were diluted 2:100 (v/v) with CW and the ZP was measured using a DTS 1060 Malvern cuvette at 22 °C without equilibration.

2.4. Loading and entrapment efficiency

The drug loading efficiency (LE%) or the amount of drug loaded in the TFS was determined by adapting a previously described method [36]. Curcumin-loaded TFS were centrifuged for 10 min at 13,000 rpm at 4 °C (Eppendorf, Germany) to remove any large crystals or aggregates of the unentrapped drug. The supernatant was diluted with isopropyl alcohol (IPA) and sonicated for 30 min (Cole-Palmer, USA). Curcumin was quantified in the supernatant to determine the actual amount of drug loaded by measuring the fluorescence intensity (excitation: 485/20 nm; emission: 535/20 nm; Spectramax i3x; Molecular Devices, USA). A curcumin standard curve was plotted using seven standards with concentrations ranging from 0.025 to 5 μg/ml and the linearity, specificity, precision and accuracy of the method were confirmed [38,39]. The LE% was calculated using the equation below [36]:

$$LE\% = \frac{actual\ \ amount\ \ of\ \ drug\ \ loaded}{theoretical\ \ amount\ \ of\ \ drug\ \ loaded} \times 100$$

The entrapment efficiency (EE%) was measured by the ultracentri-

fugation method [40] that has previously been applied to calculate curcumin EE% in ethosomes and TFS [41]. The centrifuged TFS were divided and ultracentrifuged (Sorvall wX + Ultra s, Thermofisher, USA) twice for 1 h at 40,000 rpm and 4 °C. The free drug in the supernatant was quantified as described above. The EE% was calculated using the equation below [42].

$$EE\% = \frac{actual\ amount\ of\ drug\ loaded - free\ drug}{actual\ amount\ of\ drug\ loaded} \times 100$$

2.5. In vitro release

Curcumin release from TFS was determined using a cellulose acetate dialysis bag (MWCO 12,000–14,000; Fisherbrand, UK) by enclosing 1 ml of the TFS formulation in a pre-swollen dialysis bag and suspending it in 200 ml of phosphate-buffered saline (PBS; pH 5.5) with 0.5 % (w/v) Tween 80 stirred at 300 rpm and maintained at a temperature of 32 °C. A 1 ml aliquot was withdrawn and replaced with fresh buffer at 1, 2, 3, 4, 5, 6, 8, 12, 24, 28, 48 and 72 h and the curcumin content was analysed using HPLC-UV, as described previously by Tolentino et al. [43]. Samples with curcumin content below the lower limit of quantitation (LLOQ) by HPLC were further analysed spectrophotometrically, as described above. The cumulative drug release was plotted against time and the *in vitro* release data was fitted to the modified Korsmeyer-Peppas equation proposed by Kim and Fassihi [44] to obtain the drug transport constant (K) and the transport exponents (n) of the TFS using the equation below:

$$\frac{M_t}{M_\infty} = Kt^n + b$$

Where, M_t/M_∞ represents the fractional permeated drug, t is the time, b is the possibility of a burst effect, K is the transport constant (dimension of time^{-1}), and n is the transport exponent (dimensionless) [45].

2.6. Ex vivo precorneal retention

Precorneal residence of the formulations was compared using the "OphthalMimic model" described by Barbalho et al. [46]. The model consists of a reusable support base designed to oscillate between 0° and 50° to replicate eyelid movement. A polymeric membrane, prepared by casting PVA, gelatin, type II porcine mucin and poloxamer, was affixed on the support base to mimic the ocular surface, while a commercial peristaltic pump was integrated with the platform to simulate tear flow at a rate of 1.0 ml/min for 5 min (32 movements/min). Simulated tear fluid (STF) was prepared using 0.2 % $NaHCO_3$, 0.67 % NaCl and 0.008 % $CaCl_2$, as described previously [47]. Precorneal retention was compared by placing 300 μl of each formulation on the polymeric membrane and subjecting it to simulated tear flow. The drained tear fluid was collected after 5 min and quantified for curcumin using the spectrofluorometric method described above. Statistical comparison was performed using an unpaired *t*-test (GraphPad Prism version 9.3.1).

2.7. Bovine corneal opacity and permeability assay

The bovine corneal opacity and permeability (BCOP) assay recommended by the Organisation for Economic Co-operation and Development (OECD) [48–50] was modified to evaluate the corneal biocompatibility of the test formulations. Briefly, freshly harvested bovine eyes were incubated for 10 min at 32 ± 0.5 °C and one drop of STF was added inside a centrally placed custom-made polycarbonate corneal sleeve. Eyes were incubated for 5 min before applying 150 μl of the test formulations (MCT, blank TFS, 1 % w/v Tween 80) and incubating for another 5 min. As per the OECD guideline, Milli-Q water was used as the negative control, while acetone, 5 % w/v benzalkonium chloride (BAK) and 0.1 M sodium hydroxide (NaOH) were used as positive controls. After 5 min of exposure to the test formulations, the polycarbonate sleeves were removed, and the eyes were rinsed with approximately 10 ml of warm PBS (32 ± 0.5 °C) before further incubation for 1 min. The extent of corneal damage, if any, was evaluated by observing corneal opacity and epithelial detachment. A sodium fluorescein solution (4 mg/ml; pH 7.4) was applied to ascertain the integrity of the corneal epithelium using a Burton lamp (G. Nissel & Co. Ltd., UK). Observations were graded according to individual numerical scores for corneal opacity, corneal staining (epithelial integrity) and epithelial detachment and the mean cumulative score from three eyes was used to determine the irritation potential as described previously [51,52].

2.8. Ex vivo penetration studies

Ocular distribution of curcumin from TFS formulations containing 1 mg/ml curcumin was evaluated using an ex vivo porcine eye model [53–55]. A 1 mg/ml solution of curcumin in MCT was used as the oily control. Porcine eyes were collected from the abattoir (DaHua Supermarket, New Zealand) and transported to the laboratory in cold PBS. All eyes were inspected for corneal damage or lacerations and only healthy eyes were used for penetration studies after trimming off excess tissue surrounding the eyes.

The porcine eye model was set up by placing the eyes into 6-well microplates lined with a non-absorbent lint-free sheet (DAY-LEE™, Johnson & Johnson Medical, USA) soaked in Hank's Balanced Salt Solution (HBSS; ThermoFisher Scientific, New Zealand). Custom-made polycarbonate corneal sleeves with an internal diameter of 18.5 mm (manufactured by the University of Auckland Biomedical Engineering Workshop, New Zealand) were placed on top of each eye, such that the cornea and bulbar conjunctiva were exposed to the test formulation. Excised eyelid tissue was placed on top of each eye with the tarsal conjunctiva facing the cornea.

Eyes were incubated at 35 ± 3 °C and after equilibration for 15 min, 300 μl of the test formulation (n = 3) was applied between tarsal conjunctiva and cornea. After 15 min, the eyes were rinsed and washed with HBSS to remove any excess formulation and the cornea, bulbar conjunctiva along with the sclera, and the eyelid tissue with the tarsal conjunctiva were carefully excised and fixed in Tissue-Tek® O.C.T. compound (Sakura® Finetek, USA). The tissues were sectioned (Cryo-Star NX50, Thermo Scientific, USA) to a thickness of 10 μm.

2.8.1. Corneal distribution by confocal microscopy

Curcumin distribution in the corneal epithelium and stroma was qualitatively evaluated using a confocal laser scanning microscope (FV1000, Olympus, Japan). Tissue sections were prepared as described above and cell nuclei were counterstained with 4′,6-diamidino-2-phenylindole (DAPI; Sigma-Aldrich, USA).

2.8.2. Corneal and conjunctival penetration by fluorescence microscopy

Drug penetration into the cornea, bulbar and tarsal conjunctiva was semi-quantitatively [56,57] evaluated by observing tissue sections under a fluorescent microscope (Apotome.2, Zeiss, Germany) within 6 h of sectioning. A 475 nm LED laser with laser intensity of 25% was used to illuminate the tissue sections and the signal was collected using the camera objective (20× 0.5 Axiocam 506, Zeiss Germany). The built-in green fluorescence filter (FITC-109; BP 450–490/BS495/BP 500–500) with an exposure time of 1000 ms and 100% intensity was used for all analyses.

For each corneal sample, 12 sections from the central and peripheral regions were imaged at five positions each, resulting in a total of 120 images for each eye. For the bulbar conjunctiva, 12 sections were imaged at the limbus. Meanwhile, for eyelid samples, 12 sections from the central region were imaged at three positions.

2.8.3. Digital image analysis

Curcumin penetration into ocular tissues was evaluated by digital image analysis as per the method previously described by Pelikh et al.

[56] and optimized for corneal penetration by Raab et al. [57] using Image J software version 1.8.0 [58,59]. Prior to analysis, all images were scaled using the scale function of the software to synchronize the scale bar to a specific number of pixels. The scale was set to 2.84 pixels/μm for images with a 200-fold magnification. The amount of curcumin penetrated was then determined semi-quantitatively by analysing the mean grey value per pixel (MGV/px) in each image. The higher the MGV/px (i.e. total intensity of detected light within the image), the more curcumin penetrated. The maximal penetration depth was determined manually by measuring the distance between the superficial tissue surface and the most distant pixel (corresponding to maximally penetrated curcumin) for each section.

2.8.4. Statistical analysis

Statistical comparison was performed using GraphPad Prism version 9.3.1. The total amount of curcumin penetrated and the mean penetration depth were compared by a two-way analysis of variance (ANOVA) test, followed by post hoc Šídák's multiple comparisons tests. A p-value < 0.05 was defined as statistically significant. Error bars in the figures represent the standard deviations.

3. Results and Discussion

3.1. Particle size, polydispersity index and zeta potential

The particle size, measured as Z-average, and PDI of the blank TFS were 117 ± 0.84 nm and 0.41 ± 0.004, respectively (Table 1). The measured particle size was comparable to that previously reported by Ahad et al. [33], who prepared Phospholipon 90 G and Tween 80 TFS and measured the particle size by both DLS and transmission electron microscopy. Curcumin precipitation was evident when drug loading was greater than 7.5 % w/w; therefore, LP4 (10 % w/w) and LP5 (15 % w/w) formulations were not evaluated any further. TFS having a drug loading of 2.5, 5 and 7.5 % w/w showed a 20 % increase in particle size compared to blank TFS, although the average particle size remained less than 150 nm. In line with previous literature [35,60], we observed a significant reduction in particle size and PDI after sonication. The small vesicle size obtained in this study is highly desirable as nanoparticulate formulations with a particle size of less than 200 nm are known to significantly enhance ocular drug delivery [61]. Meanwhile, the PDI of the drug-loaded TFS was considerably lower than that of blank TFS suggesting that curcumin loading stabilizes the TFS, likely due to incorporation of curcumin into the lipid bilayer of the TFS. Moreover, an increase in curcumin loading from 2.5 to 7.5 % resulted in smaller size and lower ZP values. The narrow particle size distribution of the formulations is anticipated to increase TFS stability while optimising the release kinetics [62].

The ZP of the TFS was slightly negative and in agreement with that previously observed for curcumin TFS [63]. Changes in ZP of similar vesicles loaded with different drug entities are typically observed due to the incorporation of the drug molecules in the TFS bilayer, leading to modification of the surface charge of the vesicle [41]. It has been suggested that curcumin tends to induce conformation changes of phospholipid head groups at the surface of vesicles which contribute to the negative zeta potential values [64]. Furthermore, the zeta potential of Tween 80-containing TFS tends to be negative due to partial hydrolysis of the polyethylene oxide head groups [33]. The TFS are composed of Tween 80 and phospholipids combining two stabilization principles: the phospholipid provides electrostatic stabilization while Tween 80, which is a non-ionic surfactant, provides steric stabilisation [65,66]. Our results suggest that these mechanisms superimpose to create an intermediate ZP (Table 1) for the prepared TFS. Together the phospholipid and Tween 80 bilayer displays steric and electrical hindrance, which tends to inhibit aggregation and enhances dispersion stability [67].

Table 1
TFS characterization.

TFS #	Drug loading (%)	Size [nm]	PDI	ZP [mV]	LE [%]	EE [%]
LP0	0	117 ± 0.84	0.41 ± 0.004	–	–	–
LP1	2.5	144 ± 2.23	0.09 ± 0.03	−17 ± 2.02	61.85 ± 6.12	>99.96
LP2	5.0	143 ± 1.16	0.09 ± 0.02	−14 ± 0.69	84.86 ± 4.39	>99.96
LP3	7.5	138 ± 0.89	0.12 ± 0.01	−14 ± 0.94	91.02 ± 3.33	≥99.96

3.2. Loading and entrapment efficiency

The LE% of the TFS increased as the drug loading was increased from 2.5 to 7.5 % (Table 1). This may be attributed to the hydrophobic nature of curcumin. It may be hypothesized that as drug loading is increased, the fraction of drug lost during the washing and dilution steps decreases due to limited solubility of curcumin. Drug leakage in the supernatant appeared to be minimal and the EE% was at least 99.96% for all TFS. Since the hydrophobic nature of curcumin limits its solubility in the aqueous medium used for hydrating the TFS, it may be anticipated that the drug was predominantly localised in the lipid bilayers. In the case of LP1 and LP2, no curcumin was detected in the supernatant. As such, accounting for the LLOQ of the analytical method, the EE% was estimated to be > 99.96%. For LP3, the curcumin concentration in the supernatant was just at the threshold of the LLOQ suggesting that the EE% of LP3 at 99.96% was slightly lower than that of LP1 and LP2. To minimise the risk of precipitation on storage, the LP2 formulation was used for further in vitro and ex vivo studies.

3.3. In vitro release

In vitro release of curcumin from TFS was evaluated using the dialysis bag method with PBS adjusted to pH 5.5 as the release medium since curcumin rapidly degrades at neutral-alkaline pH [68]. Moreover, 0.5% w/v Tween 80 was added to the release medium to facilitate curcumin solubilization and maintain sink conditions [38]. A triphasic release profile characterized by three distinct phases, an initial burst phase, followed by a second slower lag-phase and a final faster release phase [69,70], was observed (Fig. 1).

The *in vitro* drug release data was fitted to the Korsmeyer–Peppas equation [71] with Kim and Fassihi's [44] expression for burst effect to further elucidate the release kinetics. This model was found to be a good fit with an R^2 of 0.9892. The value of n was 0.71, which corresponds to a non-Fickian transport mechanism [71]. The high k and b values (k = 0.88; b = 0.5) suggest that after the initial burst release curcumin was released from the TFS bilayer in a more controlled manner.

Burst release is typically attributed to non-encapsulated drug particles adhered to the carrier surface or rapid hydration of easily accessible drug molecules close to the carrier surface [72]. A short burst release phase lasting 15 min was observed in which less than 2% of the total curcumin was released from the TFS. The relatively small burst release is particularly desirable for ocular drug delivery as it can minimise tear fluid dilution and drainage due to reflex tearing and can be attributed to the narrow size distribution, high EE% (>99.96%) and hydrophobic nature of curcumin, due to which it resists hydration [62]. After the initial burst release, a "lag phase" with almost negligible drug release was observed until the 2 h timepoint, which may be attributed to temporary depletion of the drug close to the TFS surface [70]. The relatively short lag phase in this study can be attributed to the presence of the edge activator in the TFS which imparts fluidity to the lipid bilayer, leading to re-arrangement of the lipid structure and modification of the diffusion barrier's robustness [70]. After the 2 h timepoint, a short "second burst", signifying the onset of erosion, followed by the final sustained release phase was observed, which may be attributed to the continuing erosion

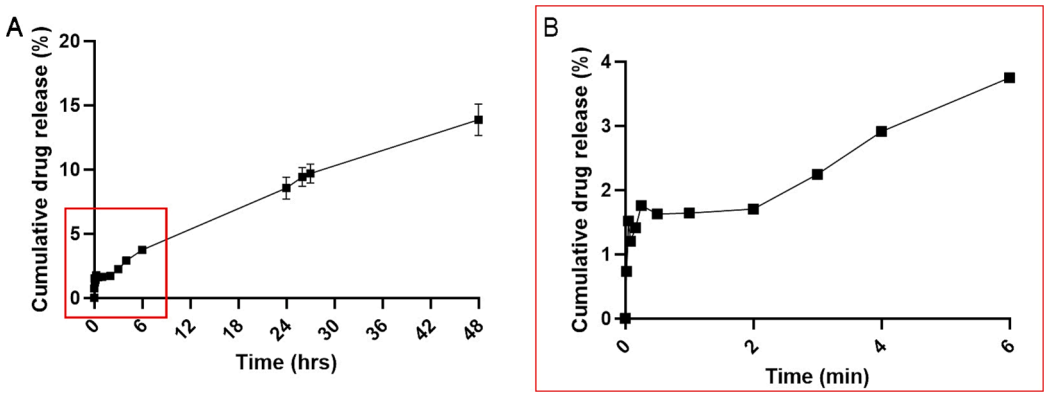

Fig. 1. A. In vitro curcumin release from transferosomes (TFS) over 48 h. B. The inset shows cumulative drug release in the first 6 h.

of the TFS by lipid hydrolysis [73,74].

3.4. Ex vivo precorneal retention

The precorneal residence of TFS compared to the oily control eyedrop was evaluated using the ex vivo "OphthalMimic model" previously developed and characterised by Barbalho et al. [46]. The OphthalMimic model simulates precorneal tear flow and blinking using perfusion pumps and rocking motion, respectively. Since this study intended to evaluate precorneal retention purely due to the adhesive nature of the TFS, no additional viscosity building or gelling agents were included in the TFS eyedrop. Over the 5 min test period, more than 79.3 ± 6.7% of the TFS formulation was drained away (Fig. 2). However, the amount of drug drained after 5 min was still comparable to that of 16% poloxamer gels reported previously using the same model [46].

Meanwhile, for the non-aqueous oily control solution, precorneal retention was significantly higher. Only 24.8 ± 1.5% of curcumin in the oily control formulation was drained away after 5 min, evidently due to immiscibility of MCT with the tear fluid.

3.5. Bovine corneal opacity and permeability assay

The BCOP assay, recommended as a more reproducible and ethical alternative to the Draize Test by the OECD [75,76] was used to evaluate corneal tolerability of the test formulations. Corneal opacity, typically indicative of corneal oedema, vacuolation and protein denaturation [77], or fluorescein staining, indicative of epithelial compromise [78], were not observed with the TFS, oily control or STF (Fig. 3). The corneal epithelium remained smooth, and no wrinkling of the epithelium was evident demonstrating biocompatibility of both formulations. The cumulative score assigned to all test formulations was 0.0 suggesting that they did not have any acute toxicity and were "practically non-irritating" on the ocular surface. Meanwhile, all of the positive controls were severely irritating with intense fluorescein staining, opacity and epithelial wrinkling and/or rupture.

3.6. Ex vivo penetration

Curcumin penetration in the cornea, bulbar and tarsal conjunctiva was evaluated by measuring the total amount of curcumin penetrated, as well as the penetration depth. Since one of the primary aims of this study was to compare TFS penetration in different ocular tissues, no polymeric

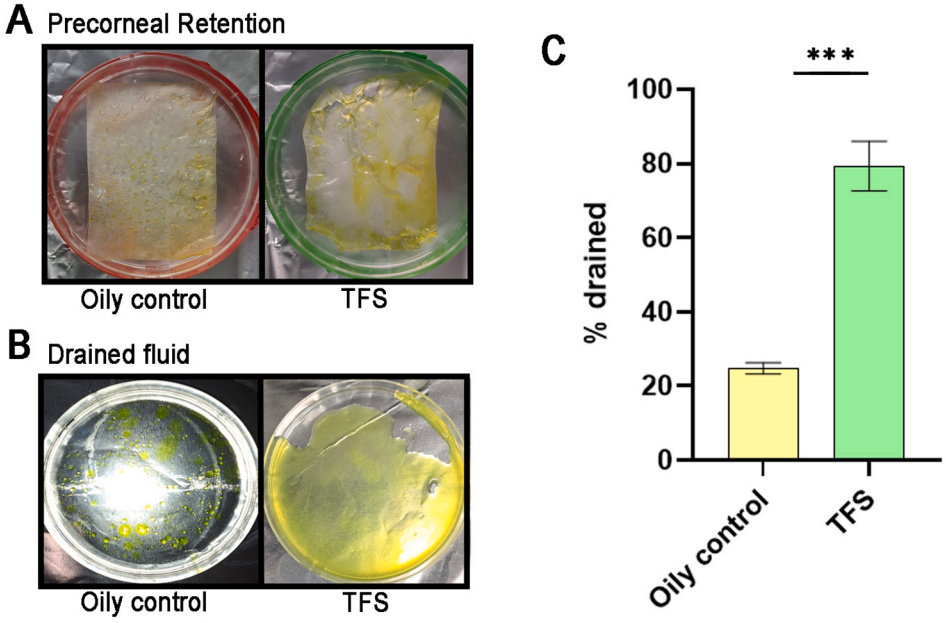

Fig. 2. Evaluation of TFS and the oily control using the "OphthalMimic" set-up. A. Precorneal retention on polymeric films, B. drained simulated tear fluid, and C. comparison of percentage drained after 5 min.

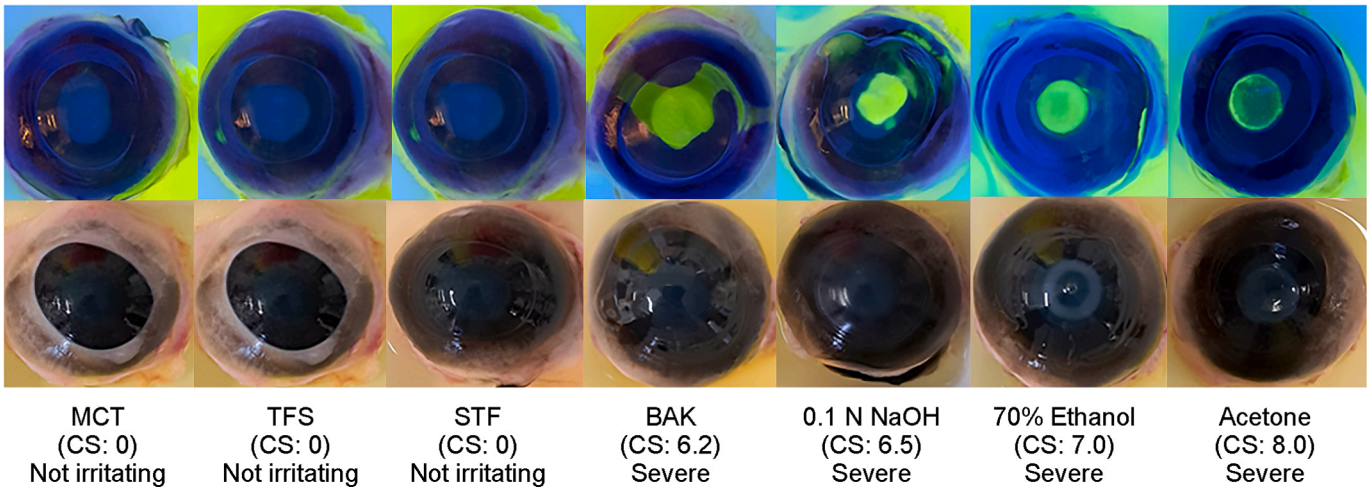

Fig. 3. Bovine corneal opacity and permeability study showing fluorescein staining (top row) and corneal opacity (bottom row) of the test formulations and controls (negative control: STF; positive controls: 5 % w/v BAK, 0.1 N NaOH, 70 % ethanol and acetone); CS = cumulative score.

or gelling agents were included in the vehicle, thus maintaining non-occlusive conditions on the ocular surface and ensuring continuous transport of TFS along osmotic gradients in the corneal and conjunctival tissue. As anticipated, significantly greater and deeper curcumin penetration, as denoted by the Total Amount Penetrated and Mean Penetration Depth, respectively, was observed from the TFS formulation in all three ocular tissues (Fig. 4).

In the cornea, the total amount of curcumin penetrated from TFS (8 ± 0.6 MGV/px) was more than two-fold greater than that observed with the oily control (3 ± 0.3 MGV/px). The cornea is believed to be the major pathway for ocular drug penetration and is composed of a superficial 5 – 7 layer thick hydrophobic epithelium with annular tight junctions that limit the entry of most drugs [18,19]. Due to its hydrophobic nature, the epithelium tends to retain hydrophobic drugs (log D > 3), such as curcumin. These hydrophobic drugs typically form a reservoir in the epithelium with sustained drug diffusion into the stroma being driven by the epithelial layer concentration gradient [79,80]. In line with previous literature showing epithelial localisation of hydrophobic drugs [54,55], confocal microscopy images (Fig. 5) showed that curcumin fluorescence was predominantly localised in the corneal epithelium after application of both test formulations. On application of the conventional oily control solution, a thin oily film was observed on the corneal surface (white arrows in Fig. 5) with the majority of the drug being localised within the oily film and in the superficial epithelial layers. Meanwhile, significantly greater curcumin penetration was observed with TFS (Figs. 4 and 5). The mean penetration depth achieved with the TFS formulation (57 ± 7.5 μm) was approximately 1.6-fold greater than that observed with the oily control (36 ± 9.2 μm) with some curcumin fluorescence also being evident in the hydrophilic stroma.

The total amount of curcumin penetrated (MGV/px) from the oily control solution into the bulbar and tarsal conjunctiva was comparable to that observed in the cornea. However, the TFS showed a more pronounced penetration enhancing effect in conjunctival tissues than in the cornea. In the bulbar conjunctiva, the total amount of curcumin penetrated from TFS (12 ± 0.8 MGV/px) was four-fold greater than that observed with the oily control (3 ± 0.3 MGV/px). Meanwhile, in the tarsal conjunctiva, the total amount of curcumin penetrated from TFS (16 ± 2.9 MGV/px) was 2.5-fold greater than that observed with the oily control (3 ± 0.8 MGV/px).

The conjunctival epithelium is more hydrophilic with 230-fold larger intercellular spaces than those in the cornea [20,21], thus it is likely to be more amenable to intercellular transport of TFS. Underlying the bulbar conjunctiva is the sclera, which is primarily composed of dense bundles of collagen, elastic fibres, fibroblasts, proteoglycans and glycoproteins, and approximately 70 % of water [81]. For most drugs, scleral penetration is typically comparable to conjunctival penetration, but greater than corneal penetration [82] as scleral transport is typically mediated via passive diffusion through aqueous media and perivascular pore pathways [82]. In previous studies, TFS have been used to enhance transdermal drug penetration since their lipid bilayers are inherently resistant to dehydration and tend to migrate along the osmotic gradient into more hydrophilic regions of the dermis [5,10]. Our results suggest that the hydrophilic conjunctiva facilitates a thermodynamically more favourable interaction with the TFS lipid bilayer than the cornea, encouraging greater and deeper drug penetration. The mean penetration depth of curcumin into the bulbar conjunctiva from the TFS (70 ± 15.1 μm) was approximately 14-fold greater than that observed from the oily control (5 ± 3.8 μm). This may be attributed to the osmotic gradient driven diffusion of TFS from the bulbar conjunctiva into the sclera suggesting that the conjunctival-scleral pathway can potentially serve as a significant complementary pathway for TFS distribution into the iris, ciliary body, uvea, choroid and the retinal pigment epithelium [17]. It should be noted, however, that since the conjunctiva is highly vascular, non-productive drug absorption into the systemic circulation may be significant [17,83]. Our ex vivo drug penetration model cannot replicate this systemic loss, leading to some overestimation in the results. Nevertheless, it provides a robust tool for comparison of drug penetration from different pharmaceutical formulations.

In comparison to the cornea and bulbar conjunctiva, significantly deeper curcumin penetration was observed from both formulations into the tarsal conjunctiva. The mean penetration depth of curcumin from the TFS formulation (83 ± 14 μm) was approximately 1.3-fold greater than that observed with the oily control (64 ± 19.5 μm). The tarsal conjunctiva tightly adheres to the tarsus and its cell morphology differs considerably from that of the bulbar conjunctiva [84,85]. The tarsal plate is a thick plaque of dense, collagenous connective tissue which also contains specialised sebaceous glands, called meibomian glands, that secret meibum lipids that are rich in fatty acids and triglycerides [86,87], which may have facilitated the uptake of hydrophobic curcumin. Asano et al. [88] have previously shown that hydrophobic drugs can achieve significantly greater concentrations in the lid margin and tarsal conjunctiva with gradient driven diffusion into the meibomian glands being several folds greater than that observed for hydrophilic drugs. Furthermore, based on their observations, they hypothesized that the barrier function of the tarsal plate was similar to that of the cornea, although peak drug concentrations in the cornea were several folds lower, likely due to tighter intercellular junctions in the corneal

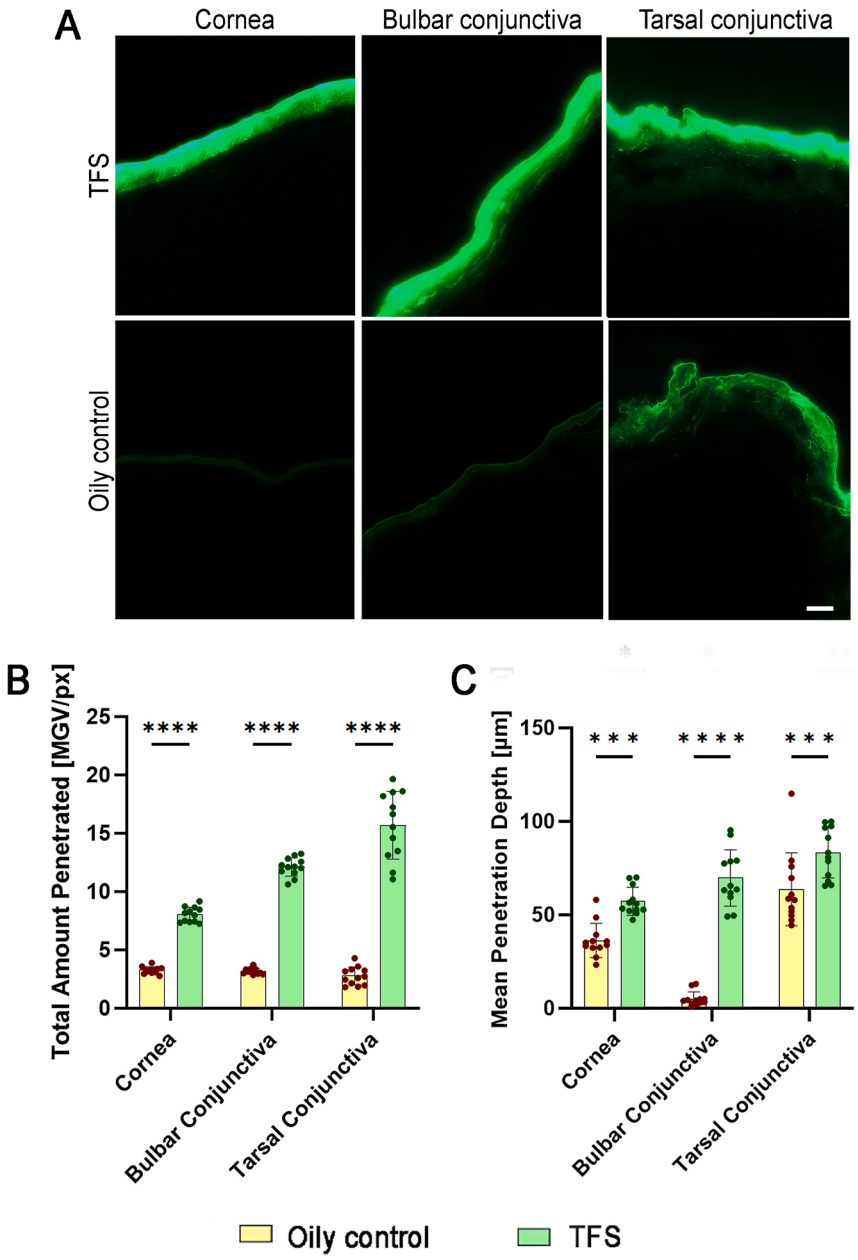

Fig. 4. Curcumin penetration from TFS and the oily control was compared using an ex vivo porcine eye model. A. Drug penetration was evaluated by observing curcumin fluorescence (green) in the cornea, bulbar and tarsal conjunctiva under a fluorescent microscope (scale bar = 50 μm). Images were digitally processed to calculate B. the total amount of drug penetrated into each tissue and C. the mean penetration depth. Statistical significance is denoted as ***: $p \leq 0.001$ or ****: $p \leq 0.0001$ (mean ± SD; data points represent the averaged results from 3 eyes). (For interpretation of the references to colour in this figure legend, the reader is referred to the web version of this article.)

epithelium. These results are in line with the observations made in the present study which shows considerably greater and deeper penetration in the tarsal conjunctiva and eyelid than in the cornea. This was especially the case with TFS which tend to migrate along osmotic gradients that are evidently stronger in the tarsal conjunctiva lining the eyelid.

It should be noted that our penetration model lacked a continuous tear clearance system, which can potentially modulate osmotic gradients on the ocular surface and influence drug penetration. Therefore, further studies evaluating the influence of continuous tear flow over a prolonged period may shed more light on the mechanism of drug transport using TFS.

3.7. Concluding remarks

In conclusion, TFS present a promising alternative for ocular delivery of hydrophobic drugs. In this study, a TFS-based formulation of curcumin having a particle size less than 150 nm with a narrow size distribution and excellent EE% was developed and characterised. In vitro release studies showed a triphasic drug release profile with minimal burst release, demonstrating the potential application of TFS for sustained delivery of hydrophobic drugs. The TFS formulation showed good corneal biocompatibility and did not have any detrimental effect on the barrier properties of the cornea. Moreover, enhanced corneal and conjunctival drug penetration, with significantly greater and deeper drug delivery was observed with TFS in all ocular tissues.

Our study, for the first time, compared TFS penetration

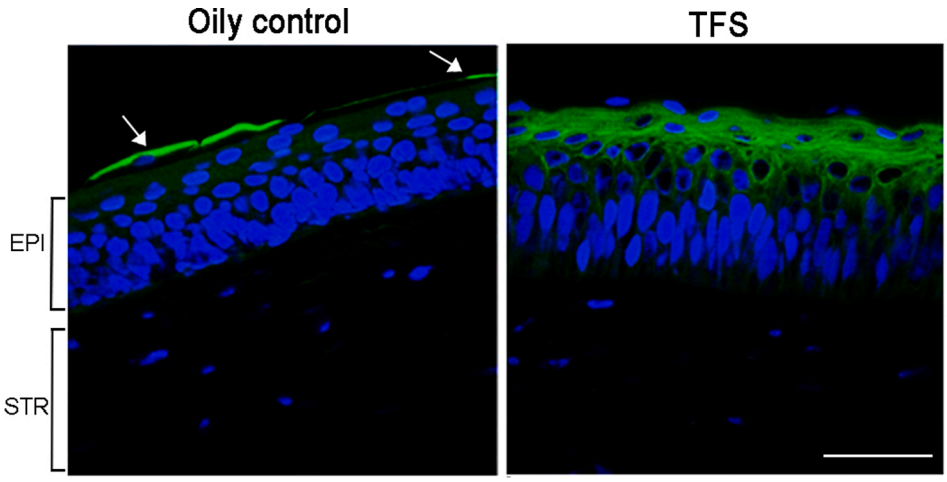

Fig. 5. Confocal microscopy images showing the distribution of curcumin (green) into the corneal epithelium (EPI) and stroma (STR) qualitatively. Cell nuclei are stained with DAPI (blue). The oily control solution formed a thin film on the corneal surface (white arrows) in which most of the curcumin fluorescence was concentrated, while TFS resulted in increased curcumin tissue penetration; scale bar = 50 μm. (For interpretation of the references to colour in this figure legend, the reader is referred to the web version of this article.)

characteristics in different ocular tissues and found that TFS penetration was greatest in the tarsal conjunctiva, followed by the bulbar conjunctiva and the cornea, respectively. Meanwhile drug penetration from the control formulation in all three ocular tissues was comparable. These observations highlight how differences in tissue morphology and osmotic gradients can impact TFS diffusion and drug bioavailability. Overall, our penetration studies suggest that TFS provide a viable alternative for ocular drug delivery and can significantly enhance the penetration of hydrophobic drugs in ocular tissues.

CRediT authorship contribution statement

Geisa Nascimento Barbalho: Writing – original draft, Validation, Methodology, Investigation, Conceptualization. **Stefan Brugger:** Methodology, Investigation. **Christian Raab:** Methodology, Investigation. **Jara-Sophie Lechner:** Methodology, Investigation. **Taís Gratieri:** Writing – review & editing, Supervision, Resources, Project administration, Funding acquisition, Conceptualization. **Cornelia M. Keck:** Writing – review & editing, Visualization, Validation, Supervision, Software, Resources, Project administration, Formal analysis, Data curation, Conceptualization. **Ilva D. Rupenthal:** Writing – review & editing, Supervision, Resources, Project administration, Funding acquisition, Conceptualization. **Priyanka Agarwal:** Writing – review & editing, Writing – original draft, Visualization, Supervision, Resources, Methodology, Investigation, Formal analysis, Data curation, Conceptualization.

Declaration of competing interest

The authors declare that they have no known competing financial interests or personal relationships that could have appeared to influence the work reported in this paper.

Acknowledgements

The authors thank the Brazilian funding agencies FAP-DF (Fundação de Apoio à Pesquisa do Distrito Federal, Brazil, Grant n. 000007462021-08), and CAPES (*Coordenação de Aperfeiçoamento de Pessoal de Nível Superior*). Priyanka Agarwal's salary was supported by Health Research Council of New Zealand project grants [20/317] and [24/741], respectively, and Ilva D. Rupenthal's directorship was funded by the Buchanan Charitable Foundation. This project was co-funded by a DAAD-PPP grant [57706981] with additional support from Education New Zealand.

Data availability

Data will be made available on request.

References

[1] J.J. López-Cano, M.A. González-Cela-Casamayor, V. Andrés-Guerrero, R. Herrero-Vanrell, I.T. Molina-Martínez, Liposomes as vehicles for topical ophthalmic drug delivery and ocular surface protection, Expert Opin. Drug Deliv. 18 (7) (2021) 819–847.
[2] R. Agarwal, I. Iezhitsa, P. Agarwal, N.A. Abdul Nasir, N. Razali, R. Alyautdin, et al., Liposomes in topical ophthalmic drug delivery: an update, Drug Deliv. 23 (4) (2016) 1075–1091.
[3] S.H. Abd El-Alim, A.A. Kassem, M. Basha, A. Salama, Comparative study of liposomes, ethosomes and transfersomes as carriers for enhancing the transdermal delivery of diflunisal: In vitro and in vivo evaluation, Int. J. Pharm. 563 (2019) 293–303.
[4] R. Sapkota, D.J. Munt, A.E. Kincaid, A.K. Dash, Liposomes and transferosomes in the delivery of papain for the treatment of keloids and hypertrophic scars, PLoS One 18 (12) (2023).
[5] G. Cevc, G. Blume, New, highly efficient formulation of diclofenac for the topical, transdermal administration in ultradeformable drug carriers, Transfersomes. Biochim. Biophys. Acta (BBA) – Biomemb. 1514 (2) (2001) 191–205.
[6] R. Fernández-García, A. Lalatsa, L. Statts, F. Bolás-Fernández, M.P. Ballesteros, D. R. Serrano, Transferosomes as nanocarriers for drugs across the skin: Quality by design from lab to industrial scale, Int. J. Pharm. 573 (2020) 118817.
[7] G.M. El Zaafarany, G.A.S. Awad, S.M. Holayel, N.D. Mortada, Role of edge activators and surface charge in developing ultradeformable vesicles with enhanced skin delivery, Int. J. Pharm. 397 (1) (2010) 164–172.
[8] P. Sivannarayana, A.P. Rani, V. Saikishore, C. VenuBabu, V. SriRekha, Transfersomes: ultra deformable vesicular carrier systems in transdermal drug delivery system, Res. J. Pharm. Dosage Forms Technol. 4 (5) (2012) 243–255.
[9] R. Sachan, T. Parashar, V. Singh, G. Singh, S. Tyagi, C. Patel, et al., Drug carrier transfersomes: A novel tool for transdermal drug delivery system, Int. J. Res. Develop. Pharmacy Life Sci. 2 (2) (2013) 309–316.
[10] G. Cevc, G. Blume, Lipid vesicles penetrate into intact skin owing to the transdermal osmotic gradients and hydration force, Biochim. Biophys. Acta Biomembr. 1104 (1) (1992) 226–232.
[11] N. Matharoo, H. Mohd, B. Michniak-Kohn, Transferosomes as a transdermal drug delivery system: Dermal kinetics and recent developments, WIREs Nanomed. Nanobiotechnol. 16 (1) (2024) e1918.
[12] S.A.T. Opatha, V. Titapiwatanakun, C.R. Transfersomes, A promising nanoencapsulation technique for transdermal drug delivery, Pharmaceutics. 12 (9) (2020).
[13] O. Uwaezuoke, L.C. Du Toit, P. Kumar, N. Ally, Y.E. Choonara, Linoleic acid-based transferosomes for topical ocular delivery of cyclosporine A, Pharmaceutics. 14 (8) (2022) 1695.
[14] R. Nanda, R.S. Narang, J.K. Narang, Design and characterization of fluconazole loaded elastic liposome based gel for treatment of keratomycosis, Fabad J. Pharm. Sci. 47 (2) (2022) 161–174.

[15] E.A. Mazyed, A.E. Abdelaziz, Fabrication of transgelosomes for enhancing the ocular delivery of acetazolamide: statistical optimization, in vitro characterization, and in vivo study, Pharmaceutics. 12 (5) (2020).
[16] K.M. Hämäläinen, K. Kananen, S. Auriola, K. Kontturi, A. Urtti, Characterization of paracellular and aqueous penetration routes in cornea, conjunctiva, and sclera, Invest. Ophthalmol. Vis. Sci. 38 (3) (1997) 627–634.
[17] E. Ramsay, E.M. del Amo, E. Toropainen, U. Tengvall-Unadike, V.P. Ranta, A. Urtti, et al., Corneal and conjunctival drug permeability: Systematic comparison and pharmacokinetic impact in the eye, Eur. J. Pharm. Sci. 119 (2018) 83–89.
[18] M. Hornof, E. Toropainen, A. Urtti, Cell culture models of the ocular barriers, Eur. J. Pharm. Biopharm. 60 (2) (2005) 207–225.
[19] P. Agarwal, I.D. Rupenthal, In vitro and ex vivo corneal penetration and absorption models, Drug Deliv. Transl. Res. 6 (6) (2016) 634–647.
[20] D.H. Geroski, H.F. Edelhauser, Transscleral drug delivery for posterior segment disease, Adv. Drug Deliv. Rev. 52 (1) (2001) 37–48.
[21] K.M. Hamalainen, K. Kananen, S. Auriola, K. Kontturi, A. Urtti, Characterization of paracellular and aqueous penetration routes in cornea, conjunctiva, and sclera, Invest. Ophthalmol. Vis. Sci. 38 (3) (1997) 627–634.
[22] M. Hadipour Jahromy, M. Qomi, S. Fazelipour, N. Sami, F. Faali, M. Karimi, et al., Evaluation of curcumin-based ophthalmic nano-emulsion on atropine-induced dry eye in mice, Heliyon. 10 (7) (2024) e29009.
[23] S.H. Chung, S.H. Choi, J.A. Choi, R.S. Chuck, C.K. Joo, Curcumin suppresses ovalbumin-induced allergic conjunctivitis, Mol. Vis. 18 (2012) 1966–1972.
[24] R. Agarwal, S. Gupta, P. Agarwal, S. Srivastava, Topically applied standardized aqueous extract of Curcuma longa Linn. suppresses endotoxin-induced uveal inflammation in rats, Indian J. Exp. Biol. 51 (10) (2013).
[25] S.K. Gupta, R. Agarwal, S. Srivastava, P. Agarwal, S.S. Agrawal, R. Saxena, et al., The anti-inflammatory effects of Curcuma longa and Berberis aristata in endotoxin-induced uveitis in rabbits, Invest. Ophthalmol. Vis. Sci. 49 (9) (2008) 4036–4040.
[26] P. Suryanarayana, M. Saraswat, T. Mrudula, T.P. Krishna, K. Krishnaswamy, G. B. Reddy, Curcumin and turmeric delay streptozotocin-induced diabetic cataract in rats, Invest. Ophthalmol. Vis. Sci. 46 (6) (2005) 2092–2099.
[27] T. Mrudula, P. Suryanarayana, P. Srinivas, G.B. Reddy, Effect of curcumin on hyperglycemia-induced vascular endothelial growth factor expression in streptozotocin-induced diabetic rat retina, Biochem. Biophys. Res. Commun. 361 (2) (2007) 528–532.
[28] W. Zhu, Y. Wu, Y.-F. Meng, J.-Y. Wang, M. Xu, J.-J. Tao, et al., Effect of curcumin on aging retinal pigment epithelial cells, Drug Des. Devel. Ther. (2015,) 5337–5344.
[29] Y. Lu, M. Lin, J. Zong, L. Zong, Z. Zhao, S. Wang, et al., Highly bioavailable curcumin preparation with a co-grinding and solvent-free process, Food Sci. Nutr. 8 (12) (2020) 6415–6425.
[30] M.K. John, H. Xie, E.C. Bell, D. Liang, Development and pharmacokinetic evaluation of a curcumin co-solvent formulation, Anticancer Res 33 (10) (2013) 4285–4291.
[31] M. Bernabé-Pineda, M.T. Ramírez-Silva, M. Romero-Romo, E. González-Vergara, A. Rojas-Hernández, Determination of acidity constants of curcumin in aqueous solution and apparent rate constant of its decomposition, Spectrochim. Acta - Part A: Mol. Biomol. Spectros. 60 (5) (2004) 1091–1097.
[32] B. Wahlang, Y.B. Pawar, A.K. Bansal, Identification of permeability-related hurdles in oral delivery of curcumin using the Caco-2 cell model, Eur. J. Pharm. Biopharm. 77 (2) (2011) 275–282.
[33] A. Ahad, A.A. Al-Saleh, A.M. Al-Mohizea, F.I. Al-Jenoobi, M. Raish, A.E.B. Yassin, et al., Formulation and characterization of Phospholipon 90 G and tween 80 based transfersomes for transdermal delivery of eprosartan mesylate, Pharm. Dev. Technol. 23 (8) (2018) 787–793.
[34] M.M. Mehanna, A.M. Motawaa, M.W. Samaha, Nanovesicular carrier-mediated transdermal delivery of tadalafil: i- formulation and physicsochemical characterization, Drug Dev. Ind. Pharm. 41 (5) (2015) 714–721.
[35] Y. He, L. Luo, S. Liang, M. Long, H. Xu, Influence of probe-sonication process on drug entrapment efficiency of liposomes loaded with a hydrophobic drug, Int. J. Polym. Mater. Polym. Biomater. 68 (4) (2019) 193–197.
[36] D.A. Rodriguez de Anda, N. Ohannesian, K.S. Martirosyan, S.A. Chew, Effects of solvent used for fabrication on drug loading and release kinetics of electrosprayed temozolomide-loaded PLGA microparticles for the treatment of glioblastoma, J. Biomed. Mater. Res. B Appl. Biomater. 107 (7) (2019) 2317–2324.
[37] R.H. Müller, R. Nitzsche, B.-R. Paulke, editors. Zetapotential und Partikelladung in der Laborpraxis: Einführung in die Theorie, praktische Messdurchführung, Dateninterpretation. Colloidal drug carriers 1st expert meeting; 1995; Berlin: Wissenschaftliche Verlagssgesellschaft; 1996.
[38] A.D. Jose, K.L. Foo, G. Hu, L. Ngar, B. Ryda, J. Jaiswal, et al., Design and evaluation of curcumin-loaded poloxamer hydrogels as injectable depot formulations, Eur. J. Pharm. Biopharm. 201 (2024) 114372.
[39] C. Liu, J.J. Maran, I.D. Rupenthal, P. Agarwal, Mechanism of ocular penetration of lipophilic drugs from lipophilic vehicles, J. Pharm. Sci. (2024).
[40] A. Gonzalez Gomez, S. Syed, K. Marshall, Z. Hosseinidoust, Liposomal nanovesicles for efficient encapsulation of staphylococcal antibiotics, ACS Omega 4 (6) (2019) 10866–10876.
[41] D. Momekova, V. Gugleva, P. Petrov, Development and evaluation of curcumin-loaded vesicular carriers: impact of formulation variables, Pharmacia. 71 (2024).
[42] G. Niu, B. Cogburn, J. Hughes, Preparation and characterization of doxorubicin liposomes, Cancer Nanotechnol.: Methods Protocols. (2010,) 211–219.
[43] S. Tolentino, T. Gratieri, M. Cunha-Filho, G.M. Gelfuso, Curcumin quantification in skin and mucosa: Optimization of extraction and chromatographic method validation, J. Chromatogr. B 1217 (2023) 123623.
[44] H. Kim, R. Fassihi, Application of binary polymer system in drug release rate modulation. 2. Influence of formulation variables and hydrodynamic conditions on release kinetics, J. Pharm. Sci. 86 (3) (1997) 323–328.
[45] I.Y. Wu, S. Bala, N. Škalko-Basnet, M.P. di Cagno, Interpreting non-linear drug diffusion data: Utilizing Korsmeyer-Peppas model to study drug release from liposomes, European Journal of Pharmaceutical Sciences 138 (2019) 105026.
[46] G.N. Barbalho, M.A. Falcão, V. Alves Amaral, J.L.A. Contarato, A.M. Barbalho, G. Kaori Diógenes, et al., OphthalMimic: A new alternative apparatus without animal tissue for the evaluation of topical ophthalmic drug products, Methods. 228 (2024) 1–11.
[47] A. Rozier, C. Mazuel, J. Grove, B. Plazonnet, Gelrite®: A novel, ion-activated, in-situ gelling polymer for ophthalmic vehicles. Effect on bioavailability of timolol, Int. J. Pharm. 57 (2) (1989) 163–168.
[48] T. Nishikawa, H. Hasumi, S. Suzuki, H. Kubo, H. Ohtani, Interconversion of cyclosporin molecular form inducing peak broadening, tailing and splitting during reversed-phase liquid chromatography, Chromatographia 38 (5–6) (1994) 359–364.
[49] L.D. Bowers, S.E. Mathews, Investigation of the mechanism of peak broadening observed in the high-performance liquid chromatographic analysis of cyclosporine, J. Chromatogr. A 333 (C) (1985) 231–238.
[50] H. Abdelkader, S. Ismail, A. Hussein, Z. Wu, R. Al-Kassas, R.G. Alany, Conjunctival and corneal tolerability assessment of ocular naltrexone niosomes and their ingredients on the hen's egg chorioallantoic membrane and excised bovine cornea models, Int. J. Pharm. 432 (1) (2012) 1–10.
[51] L.H. Bruner, D.J. Kain, D.A. Roberts, R.D. Parker, Evaluation of seven in vitro alternatives for ocular safety testing, Fundam. Appl. Toxicol. 17 (1) (1991) 136–149.
[52] P. Weterings, Y.H.M. Vanerp, editors. Validation of the BECAM assay - An eye irritancy screening test. Pharmaceutisch weekblad-scientific edition; 1987: Royal Dutch Assoc Advancement Pharmacy 11 Alexanderstraat, PO BOX 30460, 2514 The Hague, Netherlands.
[53] P. Agarwal, S. Behera, I.D. Rupenthal, Ocular Distribution of Papaverine Using Non-aqueous Vehicles, AAPS PharmSciTech 22 (5) (2021) 160.
[54] P. Agarwal, D. Scherer, B. Günther, I.D. Rupenthal, Semifluorinated alkane based systems for enhanced corneal penetration of poorly soluble drugs, Int. J. Pharm. 538 (1) (2018) 119–129.
[55] P. Agarwal, J.P. Craig, S. Krösser, K. Eickhoff, S. Swift, I.D. Rupenthal, Topical semifluorinated alkane-based azithromycin suspension for the management of ocular infections, Eur. J. Pharm. Biopharm. 142 (2019) 83–91.
[56] O. Pelikh, S.R. Pinnapireddy, C.M. Keck, Dermal penetration analysis of curcumin in an ex vivo porcine ear model using epifluorescence microscopy and digital image processing, Skin Pharmacol. Physiol. 34 (5) (2021) 281–299.
[57] C. Raab, S. Brugger, J.-S. Lechner, G.N. Barbalho, T. Gratieri, P. Agarwal, et al., Utilizing an ex vivo skin penetration analysis model for predicting ocular drug penetration: A feasibility study with curcumin formulations, Pharmaceutics. 16 (10) (2024) 1302.
[58] W. Rasband, ImageJ - Image Processing and Analysis in Java. Astrophysics Source Code Library. 2012;1:06013.
[59] C.T. Rueden, J. Schindelin, M.C. Hiner, B.E. DeZonia, A.E. Walter, E.T. Arena, et al., Image J2: ImageJ for the next generation of scientific image data, BMC Bioinf. 18 (1) (2017) 529.
[60] I. Iskandarsyah, C.D.P. Masrijal, H. Harmita, Effects of sonication on size distribution and entrapment of lynestrenol transferosome, Int. J. Appl. Pharm. 12 (Special Issue 1) (2020) 245–247.
[61] K. Baba, Y. Tanaka, A. Kubota, H. Kasai, S. Yokokura, H. Nakanishi, et al., A method for enhancing the ocular penetration of eye drops using nanoparticles of hydrolyzable dye, J. Control. Release 153 (3) (2011) 278–287.
[62] N.S. Berchane, K.H. Carson, A.C. Rice-Ficht, M.J. Andrews, Effect of mean diameter and polydispersity of PLG microspheres on drug release: Experiment and theory, Int. J. Pharm. 337 (1) (2007) 118–126.
[63] N.E. Eleraky, M. El-Badry, M.M. Omar, W.M. El-Koussi, N.G. Mohamed, M. A. Abdel-Lateef, et al., Curcumin transferosome-loaded thermosensitive intranasal in situ gel as prospective antiviral therapy for SARS-Cov-2, Int. J. Nanomed. 18 (2023) 5831–5869.
[64] Z.Y. Ng, J.-Y. Wong, J. Panneerselvam, T. Madheswaran, P. Kumar, V. Pillay, et al., Assessing the potential of liposomes loaded with curcumin as a therapeutic intervention in asthma, Colloids Surf. B Biointerfaces 172 (2018) 51–59.
[65] M.N. Mohd Izham, Y. Hussin, M.N.M. Aziz, S.K. Yeap, H.S. Rahman, M. J. Masarudin, N.E. Mohamad, R. Abdullah, N.B. Alitheen, Preparation and characterization of self nano-emulsifying drug delivery system loaded with citraland its antiproliferative effect on colorectal cells in vitro, Nanomaterials 9 (7) (2019) 1028.
[66] V. Yemparala, A. Damre, V. Manohar, K.S. Singh, G. Mahajan, S. Sawant, et al., Effect of the excipient concentration on the pharmacokinetics of PM181104, a novel antimicrobial thiazolyl cyclic peptide antibiotic, following intravenous administration to mice, Results Pharma Sci. 4 (2014).
[67] M. Basha, S.H. Abd El-Alim, R.N. Shamma, G.E.A. Awad, Design and optimization of surfactant-based nanovesicles for ocular delivery of Clotrimazole, J. Liposome Res. 23 (3) (2013) 203–210.
[68] Y.-J. Wang, M.-H. Pan, A.-L. Cheng, L.-I. Lin, Y.-S. Ho, C.-Y. Hsieh, et al., Stability of curcumin in buffer solutions and characterization of its degradation products, J. Pharm. Biomed. Anal. 15 (12) (1997) 1867–1876.
[69] S. Fredenberg, M. Wahlgren, M. Reslow, A. Axelsson, The mechanisms of drug release in poly(lactic-co-glycolic acid)-based drug delivery systems—A review, Int. J. Pharm. 415 (1) (2011) 34–52.

[70] S. Manna, Y. Wu, Y. Wang, B. Koo, L. Chen, P. Petrochenko, et al., Probing the mechanism of bupivacaine drug release from multivesicular liposomes, J. Control. Release 294 (2019) 279–287.
[71] R.W. Korsmeyer, R. Gurny, E. Doelker, P. Buri, N.A. Peppas, Mechanisms of solute release from porous hydrophilic polymers, Int. J. Pharmaceut. 15 (1) (1983) 25–35.
[72] J. Wang, B.M. Wang, S.P. Schwendeman, Characterization of the initial burst release of a model peptide from poly(d, l-lactide-co-glycolide) microspheres, J. Control. Release 82 (2) (2002) 289–307.
[73] Z. J-aA, J. Pawelchak, Effect of pH, ionic strength and oxygen burden on the chemical stability of EPC/cholesterol liposomes under accelerated conditions: Part 1: Lipid hydrolysis, Eur. J. Pharm. Biopharm. 50 (3) (2000) 357–364.
[74] N.J. Zuidam, D.J.A. Crommelin, Chemical Hydrolysis of Phospholipids, J. Pharm. Sci. 84 (9) (1995) 1113–1119.
[75] OECD. Test No. 437: Bovine Corneal Opacity and Permeability Test Method for Identifying Ocular Corrosives and Severe Irritants. Paris: OECD Publishing; 2009.
[76] OECD. Test No. 438: Isolated Chicken Eye Test Method for Identifying Ocular Corrosives and Severe Irritants. Paris: OECD Publishing; 2009.
[77] F.A. Barile, Validating and troubleshooting ocular in vitro toxicology tests, J. Pharmacol. Toxicol. Methods 61 (2) (2010) 136–145.
[78] M.K. Prinsen, H.B.W.M. Koëter, Justification of the enucleated eye test with eyes of slaughterhouse animals as an alternative to the draize eye irritation test with rabbits, Food Chem. Toxicol. 31 (1) (1993) 69–76.
[79] M.R. Prausnitz, Permeability of cornea, sciera, and conjunctiva: A literature analysis for drug delivery to the eye, J Pharma Sci. 87 (12) (1998) 1479–1488.
[80] P. Agarwal, I.D. Rupenthal, Non-aqueous formulations in topical ocular drug delivery – A paradigm shift? Adv. Drug Deliv. Rev. 198 (2023) 114867.
[81] C.S. Foster, M.S. De La Maza, Structural Considerations of the Sclera. In: The Sclera. Springer New York; 1994. p. 1-32.
[82] I. Ahmed, R.D. Gokhale, M.V. Shah, T.F. Patton, Physicochemical determinants of drug diffusion across the conjunctiva, sclera, and cornea, J. Pharm. Sci. 76 (8) (1987) 583–586.
[83] A. Urtti, Challenges and obstacles of ocular pharmacokinetics and drug delivery, Adv. Drug Deliv. Rev. 58 (11) (2006) 1131–1135.
[84] J.V. Greiner, C.D. Leahy, D.A. Welter, S.L. Hearn, T.A. Weidman, D.R. Korb, Histopathology of the ocular surface after eye rubbing, Cornea 16 (3) (1997).
[85] N. Efron, M. Al-Dossari, N. Pritchard, In vivo confocal microscopy of the palpebral conjunctiva and tarsal plate, Optomet. Vis. Sci. 86 (11) (2009).
[86] S.S. Akella, J. Liu, Y. Miao, R.S. Chuck, A. Barmettler, C. Zhang, Collagen structural changes in rat tarsus after crosslinking, Transl. Vis. Sci. Technol. 10 (5) (2021) 3.
[87] C. Joffre, M. Souchier, S. Grégoire, S. Viau, L. Bretillon, N. Acar, et al., Differences in meibomian fatty acid composition in patients with meibomian gland dysfunction and aqueous-deficient dry eye, Br. J. Ophthalmol. 92 (1) (2008) 116.
[88] N. Asano, K. Ueda, K. Kawazu, Penetration route of the selective glucocorticoid receptor agonist SA22465 and betamethasone into rabbit meibomian gland based on pharmacokinetics and autoradiography, Drug Metab. Dispos. 45 (7) (2017) 826–833.